Mechanical and Thermal Characteristics and Morphology of Polyamide 6/Isotactic Polypropylene Blends in the Presence of a β-Nucleating Agent

Jie Li, Shi-Wei Wang, Wei Yang, Bang-Hu Xie, Ming-Bo Yang

State Key Laboratory of Polymer Materials Engineering, College of Polymer Science and Engineering, Sichuan University, Chengdu 610065, Sichuan, People's Republic of China

Received 20 July 2010; accepted 28 October 2010
DOI 10.1002/app.33620
Published online 22 February 2011 in Wiley Online Library (wileyonlinelibrary.com).

ABSTRACT: The mechanical and thermal characteristics and morphology of polyamide 6 (PA6)/isotactic polypropylene (iPP) blends (10/90 w/w) prepared with different processing procedures and incorporated with an aryl amide nucleating agent, a kind of β-nucleating agent (β-NA) for iPP, were investigated. The yield strength and flexural modulus of the blends decreased as β-NA was introduced into the blends, whereas the impact strength and elongation at break improved. The crystalline structures of the blends closely depended on (1) the processing conditions and (2) competition between the β-nucleating effect of β-NA and the α-nucleating effect of PA6 for iPP. Scanning electron microscopy, differential scanning calorimetry, and X-ray diffraction were adopted to reveal the microstructures of the blends. At a low β-NA content (<0.1 wt %), the α-phase iPP dominated the blends, whereas the relative content of the β-phase iPP increased remarkably when the β-NA content was not less than 0.1 wt %. The processing conditions also showed profound influences on the supermolecular structures of iPP; this resulted in different mechanical properties of the blends. As for PA6, the crystallization behavior and crystalline structure did not exhibit obvious changes, but PA6 did play an important role in the epitaxial crystallization of iPP on PA6.
© 2011 Wiley Periodicals, Inc. J Appl Polym Sci 121: 554–562, 2011

Key words: mechanical properties; nucleation; polyamides; polymer blends; thermal properties

INTRODUCTION

It has been widely accepted that the blending of polymers is a promising route to the generation of materials with combined or even new characteristics. Polyamide 6 (PA6)/isotactic polypropylene (iPP) blends have received much attention for decades. The thermal and mechanical properties (good heat resistance, strength, and impact resistance) of polyamide and the inertness to humidity and easy processing of polypropylene (PP) are well combined in PA6/iPP blends. Because PA6 and iPP are immiscible and their blends generally form heterogeneous systems that usually display poor mechanical performance because of the lack of entanglements and/or interfacial interactions between the macromolecular chains, compatibilizers, most often copolymers,[1–3] are usually used to improve the interfacial adhesion and optimize the comprehensive properties, such as the mechanical properties,[4] thermal properties,[5] rheological properties,[6] water absorption, and tribological properties,[7] of the blends.

Three well-known crystal modifications of iPP are α (monoclinic), β (trigonal), and γ (triclinic).[8] β-Nucleated iPP has received much attention because of its excellent thermal and impact resistance. When β-nucleated iPP is blended with other semicrystalline polymers, especially those with α-nucleating effects, for example, poly(vinylidene fluoride) and polyamide, the formation of β-phase iPP (β-iPP) is generally suppressed.[9–11] It was found that the compounding method and the processing temperature determined the relative content of β-iPP in β-nucleated PA6/PP alloys.[12–14] Yang et al.[14] reported that the addition of a β-nucleating agent (β-NA) at a temperature below 190°C led to a high relative content of β crystals because PA6 remained in the solid state and β-NA was mainly dispersed in the iPP matrix. At a high temperature, β-NA was distributed in the PA6 phase or at the interface of the PA6/iPP blends; this led to a low relative content of β-iPP because of the selective encapsulation of β-NA in the PA6 matrix and the α-nucleating effect of PA6 in β-nucleated PA6/PP blends.[12] They also found that the melting characteristics of iPP also varied apparently, whereas almost no difference was observed for those of PA6 with different compounding methods.

Correspondence to: W. Yang (ysjsanjin@163.com).
Contract grant sponsor: National Natural Science Foundation of China; contract grant number: 20734005.
Contract grant sponsor: Program for New Century Excellent Talents in University; contract grant number: NCET-08-0382.

© 2011 Wiley Periodicals, Inc.

To reinforce the adhesion of the PA6/iPP interface, Marco et al.[15] used PP functionalized with maleic anhydride (PP-*g*-MA) to compatibilize PA6/iPP blends and revealed the formation of a graft copolymer between PA6 and PP-*g*-MA via chemical bonding of the terminal amino group of PA6. Moreover, the use of PP-*g*-MA led to reductions in the crystallinity and crystallization rate of PA6 because of the diluent effect of the molten iPP; as for iPP, the nucleating activity of PA6 became much smaller in the presence of PP-*g*-MA because of a reduction in the segmental mobility of the PA6 molecular chains due to the grafting reactions.[16]

To further understand the interface of PA6/iPP blends, Laurens et al.[17] used spin-coating solutions on silicon wafers to prepare thin film bilayers with iPP–PA6 diblock copolymers and found an oriented epitaxial crystallization of iPP on PA6; this stabilized the interface of PA6/iPP assemblies because of the epitaxially recrystallized lamellae, which could bridge soft amorphous regions in the substrate lamellar structure. Later, they adopted syndiotactic polypropylene (sPP)/PA6 diblock copolymers as compatibilizers to study the crystalline orientation in the immediate vicinity of the PA6/PP interface and adhesion at the PA6/PP interfaces.[18] The results demonstrate an epitaxial crystallization of sPP on PA6, which was oriented in the immediate vicinity of the interface, whereas it was not sufficient by itself to promote a strong adhesion at the PA6/iPP interface because of its poor corresponding adhesion with strong epitaxy at interfaces. They suggested that the miscibility and cocrystallization of the PP block of the copolymer and the PP matrix might have been the principal factor for good adhesion between iPP and PA6.

However, the relationship between the microstructures and macroscopic properties of PA6/iPP blends has not been established systematically until now. In our study, an aryl amide nucleating agent (TMB-5) was used as a β-NA for iPP in the PA6/iPP blends with the aim of improving the compatibility of the PP and PA6 components and with the consideration that the amino group in TMB-5 could interact with the hydroxyl group in PA6 to a certain extent.

EXPERIMENTAL

Materials

All of the materials used were commercially available. iPP (T30S) was obtained from Lanzhou Petroleum Chemical (Lanzhou, Gansu, China) and had a melt flow rate of 2.6 g/10 min (ASTM D 1238, 230°C, 2.16 kg load) and an isotactic index of 98%. PA6 (trademark M2800), with a melt flow rate of 11.0 g/10 min (ASTM D 1238, 230°C, 2.16 kg load) and a density of 1.14 g/cm^3, was supplied by Guangdong Xinhui Meida Nylon Co., Ltd. (Jiangmen, Guangdong, China). The aryl amide nucleating agent TMB-5 (thermal decomposition temperature = 348.9°C) was purchased from the Fine Chemicals Department of the Shanxi Institute of Chemical Industry (Taiyuan, Shanxi, China). The diameter of the particles was in the range 120–150 nm, and their length was around 400 nm. A more detailed chemical structure of TMB-5 could not be found, but Varga and Menyhárd[19] deduced that TMB-5 has a similar chemical structure to some aromatic amine β-phase NAs, such as *N,N′*-dicyclohexyl-2,6-naphthalenedicarboxamide.

Sample preparation

The PA6 resin was dried for 12 h *in vacuo* at 80°C before processing to prevent heat oxidation degradation. To obtain a fine dispersion of β-NA in the PA6/iPP blends, a two-step blending process was adopted. For one group, called the *P1 group*, a master batch of iPP with 5 wt % β-NA was prepared with an internal mixer (XSS-300, made in Shanghai, China) first, and then, the master batch was melted with different contents of iPP and PA6 at a weight proportion of 10/90 (PA6/iPP) via an SHJ-20 corotating twin-screw extruder (made in Nanjing city, Jiangsu province, China) with a screw diameter of 25 mm, a length-to-diameter ratio of 32, and a temperature profile of 195–230°C from the feeding zone to the die to obtain the desired β-NA ratio in the blends. The extrudate was quenched in water and pelletized. After they were dried for 12 h *in vacuo* at 80°C to remove the moisture, the pellets were injection-molded into dumbbell tensile samples and standard rectangular impact samples on a PS40E5ASE precise injection molding machine (made by Nissei, Japan) with a temperature profile of 220–255°C from the feeding zone to the nozzle.

To study how the β-NA dispersed in the PA6/iPP blends when the processing procedures were different, another group of blends, called the *A1 group*, was prepared and compared with the other blends. A master batch of PA6 with 5 wt % β-NA was prepared with the internal mixer first, and the rest of the procedures were the same as those for the P1 group.

Tests and characterization

The tensile test was performed on an Instron 5567 testing machine (Canton, MA) at ambient temperature (ca. 23°C) according to ASTM D 638, and the flexural test was conducted on an AGS-J testing machine (made by SHIMADZU, Japan) according to ASTM D 790. The yield strength (σ_Y) and elongation at break (EB) were obtained from the stress–strain curves of the blends at a crosshead speed of 50 mm/min. The flexural modulus (E_f) was measured at a loading

speed of 2 mm/min. At least seven specimens were tested, and the average values are reported.

The notched Izod impact strength (σ_I) was obtained with a UJ-40 impact testing machine (Chengde Laboratory Instrument Factory, Hebei, China) according to ASTM D 256. All of the specimens were tested at ambient temperature (ca. 23°C). At least five specimens were tested, and the average values are used here.

First, the specimens were cryogenically fractured in liquid nitrogen. The fracture surfaces were etched by formic acid to remove the PA6 phase, and then, a mixed acid solution, containing 33 wt % concentrated sulfuric acid, 66 wt % concentrated phosphoric acid (H_3PO_4), and 1.3 wt % potassium permanganate,[20] was used to etch the amorphous region of iPP on the fracture surface at ambient temperature (ca. 23°C) for 16 h. The samples were gold-coated and examined via a scanning electron microscopy (SEM) device (FEI INSPECT F 50, FEI, Hillsboro, OR) with an acceleration voltage of 30 kV.

The samples for the differential scanning calorimetry (DSC) tests were taken from the core layer of the injection-molded bars. DSC scanning of the samples was performed on a TA DSC Q20 differential scanning calorimeter (New Castle, USA) in a nitrogen atmosphere. The calibration of the temperature and heat flow scales at the same heating rate was performed with standard indium. The samples were heated quickly to 240°C and held at 240°C for 5 min to eliminate any thermal history and were then cooled to 100°C at a rate of 10°C/min to determine the crystallization behavior, after which they were heated again from 100 to 240°C at a rate of 10°C/min. The thermograms were evaluated by means of Universal V2.6D (TA Instruments) software.

All of the samples used for X-ray diffraction (XRD) characterization were cut from the core layer of the injection-molded bars by an ultrathin semi-automatic microtome (KD-3358, Jinhua, Zhejiang, China), which were 1 mm away from the surface layer. Patterns of the specimens were recorded at room temperature with a Philips X'Pert Pro MPD DY1291 apparatus (PHILIPS, Netherlands), equipped with nickel-filtered Cu Kα radiation with a wavelength of 0.154 nm in the reflection mode. The operating conditions of the X-ray source were set at a voltage of 40 kV and a current of 35 mA in a 2θ range of 12–30° with a step scanning rate of 2°/min. The β-iPP fraction (K_β) was calculated according to the Turner–Jones formula:[21]

$$K_\beta = H_{300}^{\beta}/(H_{110}^{\alpha} + H_{040}^{\alpha} + H_{130}^{\alpha} + H_{300}^{\beta})$$

where H_{110}^{α}, H_{040}^{α}, and H_{130}^{α} are the intensities of the (110), (040), and (130) reflections of the α-phase iPP (α-iPP), respectively, and H_{300}^{β} is the intensity of the (300) reflection of β-iPP.

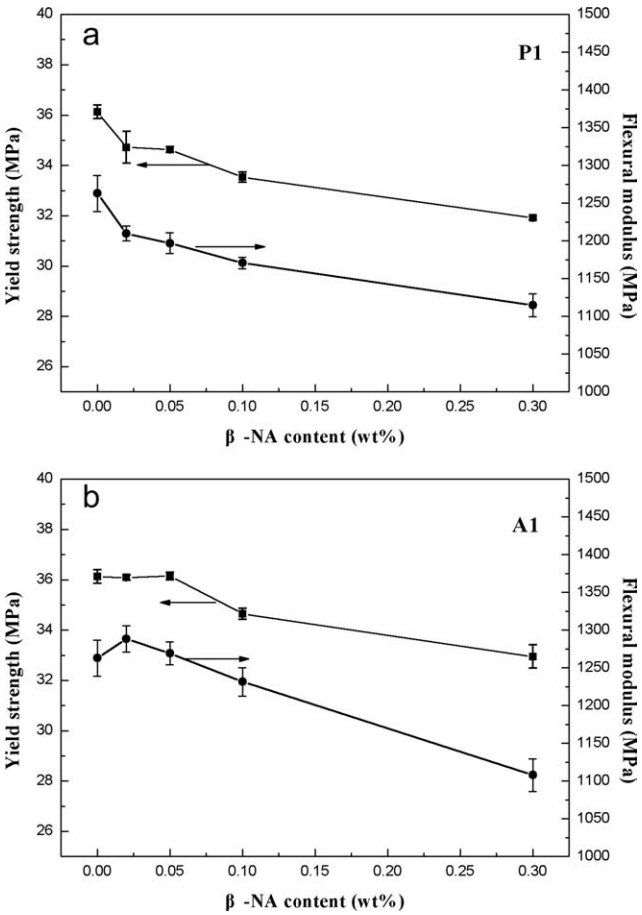

Figure 1 σ_Y and E_f versus the β-NA content in PA6/iPP blends with different processing procedures.

RESULTS AND DISCUSSION

Mechanical properties

As shown in Figure 1, whether β-NA was first melted with iPP or PA6, σ_Y and E_f of the blends decreased to a certain extent with increasing β-NA content. Nevertheless, some difference existed between the P1 and A1 groups. At a relatively low β-NA content (<0.05 wt %), σ_Y and E_f of the P1 group were lower than those of the PA6/iPP simple blend (AP1), whereas in the A1 group, they were almost the same as those of the simple blend. This phenomenon could be explained by the different distribution of β-NA in the blends of the P1 and A1 groups. In the P1 group, because β-NA was first melted with iPP, the higher melting viscosity of iPP compared with PA6 hindered the β-NA from diffusing into the PA6 phase and facilitated the formation of β crystals in the iPP matrix. As is known, σ_Y and the elastic modulus of β-iPP were lower than those of α-iPP.[22] The decreases in σ_Y and E_f of the P1 group in Figure 1 could be interpreted by the increasing content of β crystals in iPP formed in the blends and were consistent with previously reported

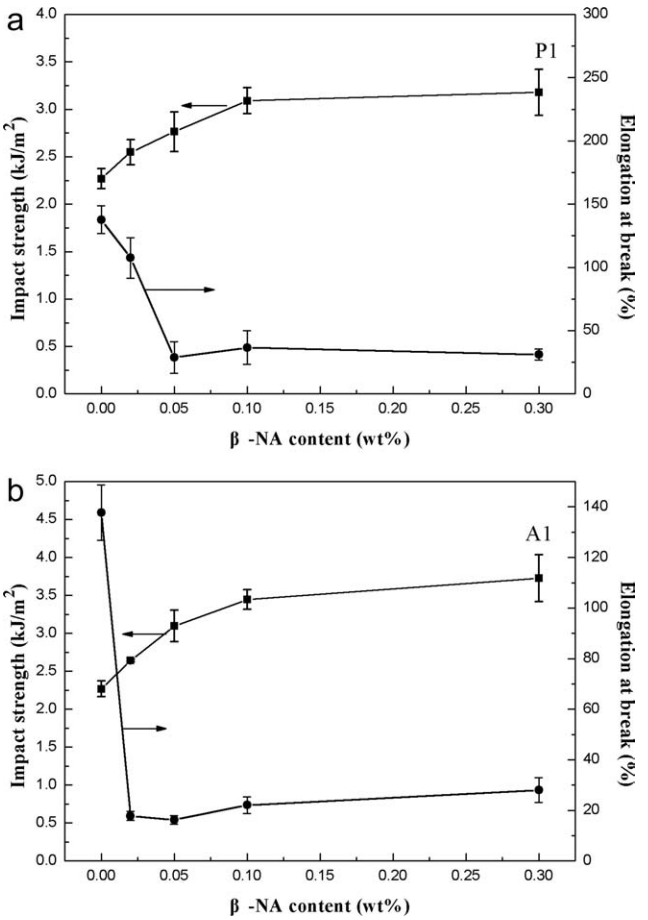

Figure 2 σ_I and EB versus the β-NA content in PA6/iPP blends with different processing procedures.

results.[23] Because the amino group in the β-NA may have caused some interactions with the hydroxyl group in the PA6 molecular chains, in the A1 group, the β-NA was encapsulated in the PA6 phase, and it was difficult for the nucleating agent to transfer into the iPP matrix. So, a relatively low content of β-NA in the PP matrix did not induce a large amount of β-iPP in the blends of the A1 group. As a result, when the content of β-NA was less than 0.05 wt %, the values of σ_Y and E_f were almost unchanged or were only a little higher than those of the PA6/iPP simple blend because of the α-nucleating ability of PA6 for iPP.

EB and σ_I of the blends are shown in Figure 2 as a function of the β-NA content. The introduction of the β-NA into the blends improved σ_I of the blends to some extent; this was consistent with the unique characteristic of β-iPP. The mechanism of the superior toughness of β-iPP was attributed to (1) the β-to-α phase transition induced by mechanical force, accompanied by the densification of the crystal transformation, which resulted in fine cavities and absorbed more energy; (2) the superior mechanical damping of β-iPP; and (3) the peculiar crystalline structure of β-iPP.[24] Because β-iPP exhibited a sheaflike structure of radial lamellae growing in bundles from a central nucleus without any epitaxial growth of tangential lamellae, the plastic deformation was not be disturbed by the physical network created by crosshatched crystallites. Concretely, the deformation of the amorphous chains (and, therefore, the lamella separation process) was facilitated in the early stages of dilatational deformation for the β form because no interlocking structure blocked their mobility; this allowed an efficient stress transfer.[24] It is generally considered that the content of β-iPP is the main factor determining the toughness of iPP; however, recently, Luo et al.[25] adopted different molten temperatures to prepare samples with constant β-NA contents and demonstrated that the paramount factor was the connection between the crystallites instead of the β-iPP content. Bai et al.[23] suggested that critical and supercritical β-NA contents led to different supermolecular structures because of its various dissolutions among the iPP matrix, such as a bundlelike morphology with a high content of β-NA and a finely dispersed form at a low content.

In this study, the value of σ_I increased distinctly when the β-NA content was less than 0.1 wt % and then grew slowly with increasing β-NA content. So, 0.1 wt % was regarded as a watershed of β-NA content in our system, below which β-NA could finely dissolve in the melt, and more β-iPP was induced with increasing β-NA content. This led to an increased impact toughness. When the β-NA content was higher than 0.1 wt %, the amount of β-iPP reached a saturate state, and the growing trend of σ_I became lower than before.

EB of P1-0.02 (the blend with a β-NA content of 0.02 wt % in the P1 group) did not drop so dramatically compared with other blends in the P1 group with a higher content of the β-NA, whereas the EB value of A1-0.02 (the blend with a β-NA content of 0.02 wt % in the A1 group) had already dropped to a quite low value. In the P1 group, the β-NA was first melted with the iPP matrix, and PA6 had a relatively lower melt viscosity, so β-NA mainly dispersed in the iPP phase, and a certain amount of β crystals were induced; this was beneficial for EB because of its fine strain properties.[22,26] As for A1-0.02, the poor EB value resulted from the following factors: (1) because the β-NA was encapsulated in the PA6 matrix, α crystals dominated in the iPP matrix because of the self-nucleating ability of iPP and the α-nucleating ability of PA6 for iPP, and (2) α-iPP was organized in a crosshatched lamellar structure, and consequently, this kind of interlocking structure stiffened the α spherulites and made the plastic gliding of α-iPP very difficult. In the blends with relatively high β-NA contents (>0.1 wt %), the

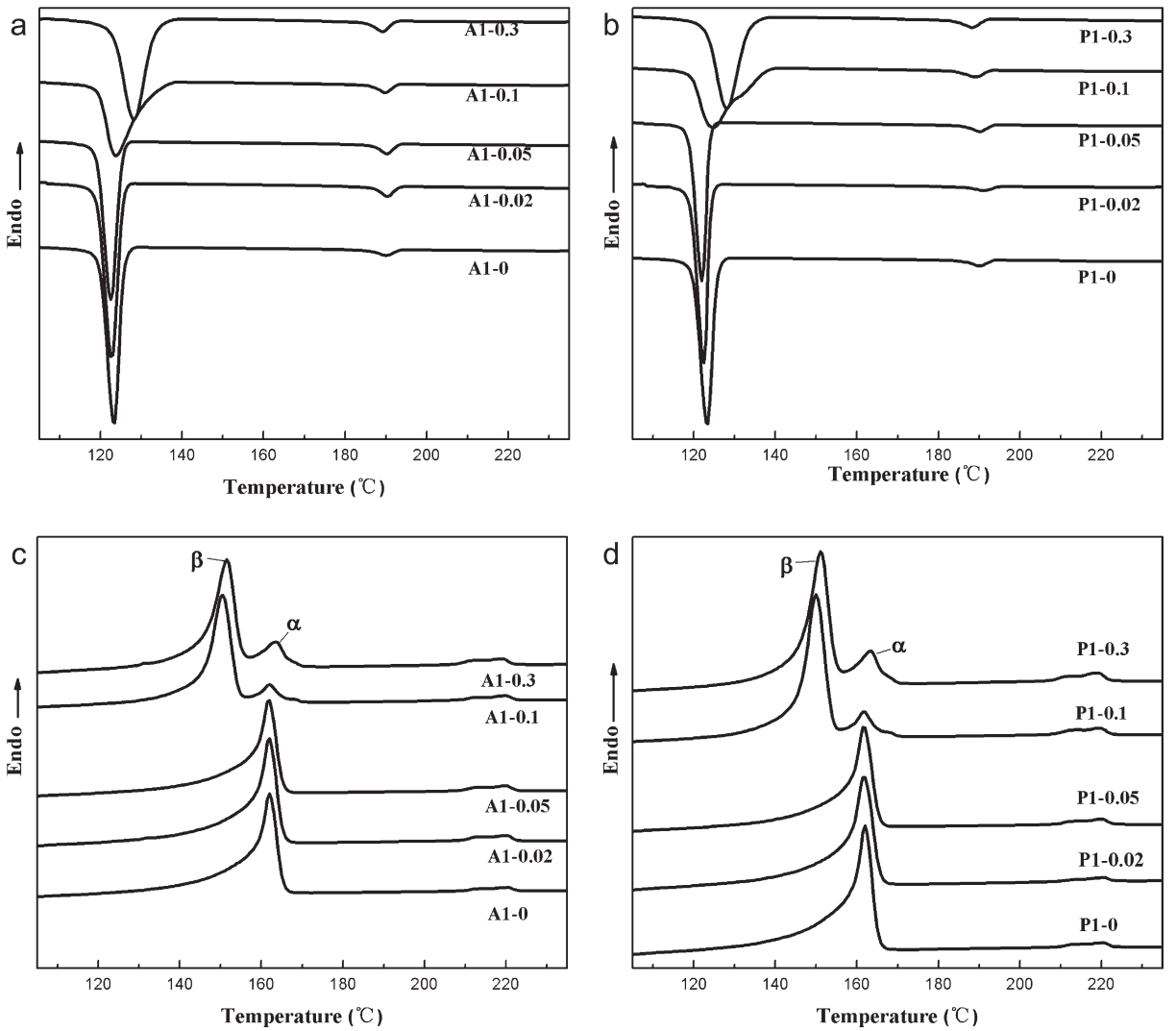

Figure 3 (a,b) DSC cooling and (c,d) melting curves of PA6/iPP blends with various β-NA concentrations.

nucleating ability of the β-NA was stronger than PA6, and β crystals emerged considerably in the iPP matrix, so it was reasonable for the blends to present a higher value of EB.

Thermal properties

The DSC cooling and heating curves of the PA6/iPP blends containing various contents of the β-NA are shown in Figure 3, and the crystallization and melting parameters are listed in Table I. Because the PA6 phase could induce the formation of α-iPP during the reheating process, we adopted a K_β calculated via the XRD results to reflect the relative content of β-iPP.

In the cooling process of the blends, when the contents of β-NA were relatively low, that is, 0.02 and 0.05 wt %, the crystallization peak (T_c) of iPP did not change much; this indicated that the α-nucleating ability of PA6 for iPP surpassed the β-nucleating ability of the β-NA and that PA6 played a crucial role in the crystallization of iPP. With increasing β-NA content, the T_c of iPP moved toward a higher temperature; this indicated overwhelming nucleating effects of β-NA versus those of the PA6 particles. Consequently, iPP could crystallize at higher temperatures and formed more developed crystals. Attention should be paid to the T_c of PA6, which decreased with increasing β-NA content, both in the A1 and P1 groups. In the melting process of the blends, β-NA was prone to transfer to the interface between iPP and the PA6 component because the β-NA we chose was a polar substance with amide groups, which had some interactions with the PA6 molecular chains; the β-NA could induce the crystal growth of iPP, which also had certain interactions with the PA6 phase. Consequently, the interaction of the β-NA between both components of the blends hindered the crystallization of PA6 and resulted in a lower T_c in PA6 in the blends.

TABLE I
DSC Crystallization and Melting Parameters of iPP in PA6/iPP Blends with Various β-NA Contents

Sample	T_c for iPP (°C)	ΔH_c for iPP (J/g)	T_m for iPP (°C)		ΔH_m for iPP (J/g)		K_β
			β	α	β	α	
AP1	123.3	86.7	—	162.0	—	95.5	—
A1–0.02	122.7	85.5	—	161.9	—	91.0	—
A1–0.05	122.5	83.3	—	161.8	—	89.7	—
A1–0.1	123.8	75.3	149.8	162.1	78.3	11.2	60.3
A1–0.3	128.2	76.3	150.6	163.1	74.5	15.8	93.8
P1–0.02	121.0	86.4	—	161.7	—	92.2	—
P1–0.05	122.0	81.1	—	161.7	—	88.5	—
P1–0.1	124.7	74.2	150.2	162.7	78.7	11.5	55.0
P1–0.3	128.1	74.5	150.4	163.1	70.5	15.4	94.0

ΔH_c is the enthalpy of crystallization and ΔH_m is the enthalpy of fusion.

In the melting process of the blends, the melting peak of β-iPP appeared in the blends at a relatively high β-NA content (>0.1 wt %), and compared with the curves of the blends containing a relatively low β-NA content (0.02 and 0.05 wt %), the peak area of α-iPP was depressed to a large extent, and the β-iPP peak appeared and dominated. The difference in the melting curves confirmed the nucleating competition between the β-NA and PA6 in both the P1 and A1 groups. Below a β-NA content of 0.1 wt %, there was no melting peak for β-iPP, and at higher β-NA contents, the β-iPP peak appeared. The α-iPP peak in the blends containing 0.1 or 0.3 wt % β-NA resulted from the transition of β to α during heating and the α-nucleating ability of PA6 during crystallization. From Table I, the melting temperature (T_m) of iPP after the addition of β-NA was almost unchanged, whereas the ΔH_m (the enthalpy of fusion) value of α-iPP declined with increasing β-NA content and decreased distinctly at a β-NA content of 0.1 wt %. This suggested that the nucleating ability of 0.1 wt % β-NA was much stronger than PA6, and during crystallization, the formation of α-iPP was inhibited to some extent. It was interesting to find that in both the P1-0.1 and A1-0.1 blends, the values of ΔH_m of α-iPP and β-iPP almost remained at the same level. This suggested that the distributions of the β-NA between the P1-0.1 and A1-0.1 blends were similar: β-NA in the PA6 phase was already in a saturated state, and the remaining β-NA was distributed in the iPP matrix and induced β-iPP at a similar content. In contrast to our expectation that in the A1 group, β-NA would have more intimate interaction with PA6, in fact, β-NA actually was not encapsulated in the PA6 matrix completely at a high content of β-NA. We presumed that in the preparation of the blends, the high content of the β-NA in the PA6 phase caused the transfer of the β-NA from PA6 toward the iPP matrix because of the saturation of β-NA in PA6; 0.1 wt % β-NA was the supersaturation value for PA6 in our system. Moreover, in the P1-0.3 and A1-0.3 blends, the increasing trend of the ΔH_m value of α-iPP resulted from the self-aggregation of the β-NA during the reheating process; this was not beneficial for iPP to form β-iPP.[22,24,25] Generally speaking, the DSC results were consistent with the results of the mechanical property and morphology observations.

Fracture morphology of the iPP matrix

To reveal the microstructures determining the mechanical properties of the blends, Figure 4 shows the cryogenic fracture morphology of the simple PA6/iPP blend and samples of the P1 group after the chemical etching of the PA6 component and the amorphous region of iPP. Because PA6 was a strong α-nucleating agent for iPP,[10–12] there was competition between the nucleating effect of PA6 and β-NA in the PA6/iPP system, and at a relatively low β-NA content (<0.1 wt %), the resulting crystal modification of iPP was mainly α modification. As clearly shown in Figure 3(a–c), the crystals in iPP were mainly α-iPP, and an epitaxial crystallization of iPP occurred around the PA6 particles. In the PA6/iPP-0.05 blend, distinct boundaries of α crystals were observed because of the interlocking structure, as shown in the box of Figure 4(c); this made the gliding of crystal lamella difficult. Consequently, the EB value of this blend was much lower than that of the PA6/iPP-0.02 blend. In Figure 4(d,e), one can clearly observe β cylindrites of iPP around PA6 and β-hedritic crystals in the iPP matrix. After the etching of PA6 and amorphous region of the iPP crystals, holes were left by the PA6 particles in the blends, and the inner surfaces of the holes became coarser than in the blends with lower contents of the β-NA; this indirectly showed that the interaction of PA6 and iPP was stronger. Moreover, around the holes left by the PA6 particles, we clearly observed

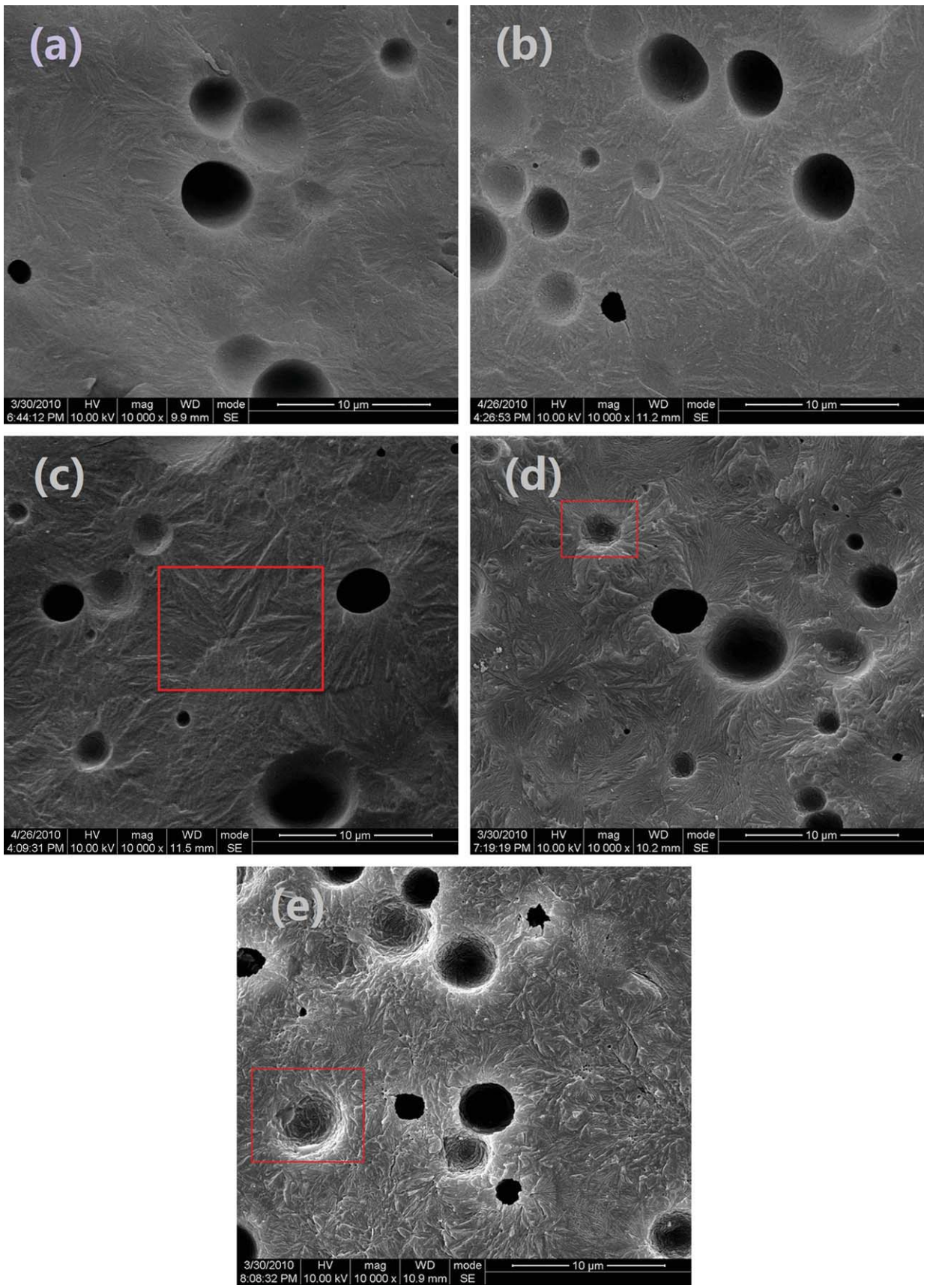

Figure 4 SEM photographs of P1 samples with different β-NA contents: (a) PA6/iPP-0, (b) PA6/iPP-0.02, (c) PA6/iPP-0.05, (d) PA6/iPP-0.1, and (e) PA6/iPP-0.3. [Color figure can be viewed in the online issue, which is available at wileyonlinelibrary.com]

the epitaxial crystallization of iPP on PA6; this was also beneficial for strengthening the interaction of the iPP and PA6 components. As a result, relatively higher values of EB of the blends were obtained.

As shown in Figure 4(d,e), the size of the β spherulites of iPP in the former one was larger than that in the latter, and the lamellar arrangement in these spherulites was distorted irregularly. The large size of the β-iPP spherulites in P1-0.1 was due to the fine dispersion of β-NA in the iPP matrix, and β-iPP axialites were obvious around PA6 in the iPP matrix, whereas, in the P1-0.3 blend, the size of β-iPP was smaller, and the areas of axialites also decreased. The different morphologies between these two blends could be credited as the self-aggregation of the β-NA at higher content of the β-NA. Luo et al.[25] and Dong et al.[26] also observed different morphologies of iPP because of the solubility and self-aggregation of a β-NA.

In this study, the morphologies of the iPP crystals relied on the following factors: (1) nucleating competition between PA6 and β-NA and (2) the solubility and self-aggregation of the β-NA. The morphologies of the A1 group were similar to those of the P1 group and are not shown here.

Crystalline structures

To reveal the microstructures of the blends, we adopted XRD to detect the differences of the blends prepared with different processing procedures. The XRD patterns of the blends are shown in Figure 5. As is consistent with the DSC results, when the β-NA content was below 0.05 wt %, the characteristic diffractions of β-iPP were not observed, whereas when the β-NA content was 0.1 wt %, the diffraction of β-iPP emerged, and the characteristic diffractions of α-iPP were restrained significantly. Moreover, when the β-NA content was 0.3 wt %, the characteristic diffractions of α-iPP almost disappeared with only strong diffractions of β-iPP left. The K_β value, as listed in Table I, increased with increasing β-NA content. For the P1-0.1 and A1-0.1 blends, the higher K_β value of A1-0.1 may have resulted from the interaction between PA6 and β-NA around the interface of the PA6/iPP blends, as we supposed; this could have prevented the β-NA from self-aggregating in the PA6 matrix when it was transported into the iPP matrix and induced the β-NA to finely disperse in the vicinity of the PA6/iPP interface, whereas in P1-0.1, the self-aggregation and inferior distribution of β-NA in the iPP matrix were the primary factors causing a lower content of β-iPP crystals. When the β-NA content was 0.3 wt %, the K_β value did not change much in either the A1 and P1 groups; this could be considered a saturation state of the β-NA in the blends.

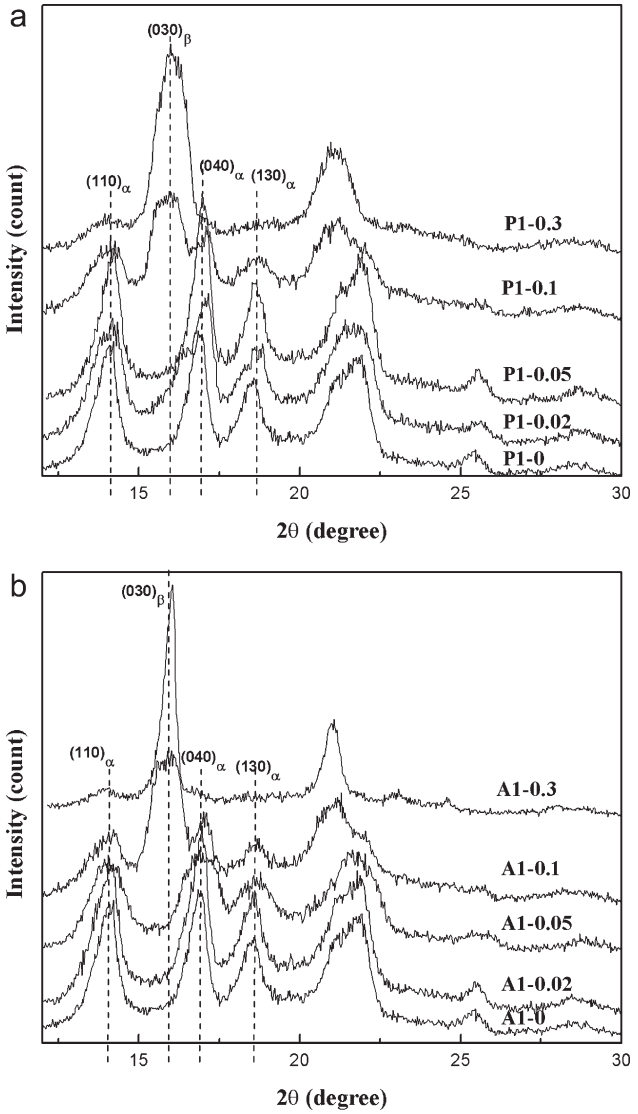

Figure 5 XRD patterns of PA6/iPP samples with different β-NA concentrations under different processing conditions.

CONCLUSIONS

The mechanical properties, thermal properties, and morphologies of β-nucleated PA6/PP blends were studied, and the results reveal nucleating competition between the β-NA and PA6 for all of the processing procedures used. At low β-NA contents (<0.1 wt %), the σ_Y and E_f values in the A1 group were nearly as great as those in the simple PA6/iPP blend because of the α-nucleating ability of PA6 for iPP, whereas in the P1 group, they decreased a little because of the β crystals induced by the β-NA. At high β-NA contents, the same level of H_m of P1-0.1 and A1-0.1 and the K_β of the P1-0.3 and A1-0.3 blends indirectly reflected the saturation states of both the PA6 and iPP matrixes, respectively.

The authors are heavily indebted to Zhu Li (Center of Analysis and Testing of Sichuan University) for careful SEM observations.

References

1. Bidaux, J. E.; Smith, G. D.; Bernet, N. J.; Månson, A. E.; Hilborn, J. Polymer 1996, 37, 1129.
2. Ohlsson, B.; Hassander, H.; Törnell, B. Polymer 1998, 39, 6705.
3. Jannerfeldt, G.; Boogh, L.; Månson, J. A. E. J Polym Sci Part B: Polym Phys 1999, 37, 2069.
4. Hsiao, K. J.; Jue, Z. F.; Kong, D. C.; Chen, F. L. J Appl Polym Sci 2006, 101, 1471.
5. Yang, W.; Li, Z. M.; Xie, B. H.; Feng, J. M.; Shi, W.; Yang, M. B. J Appl Polym Sci 2003, 89, 686.
6. Gahleitner, M.; Kretzschmar, B.; Vliet, G. V.; Devaux, J.; Pospiech, D.; Bernreitner, K.; Ingolic, E. Rheol Acta 2006, 45, 322.
7. Ohlsson, B.; Hassander, H.; Törnell, B. Polymer 1998, 39, 6705.
8. Crissman, J. M. J Polym Sci Part A-2: Polym Phys 1969, 7, 389.
9. Varga, J.; Garzó, G. Angew Makromol Chem 1990, 180, 15.
10. Varga, J.; Menyhárd, A. J Therm Anal Calorim 2003, 73, 735.
11. Menyhárd, A.; Varga, J.; Liber, Á.; Belina, G. Eur Polym J 2005, 41, 669.
12. Yang, Z. G.; Zhang, Z. S.; Tao, Y. J.; Mai, K. C. Eur Polym J 2008, 44, 3754.
13. Yang, Z. G.; Chen, C. Y.; Liang, D. W.; Zhang, Z. S.; Mai, K. C. Polym Int 2009, 58, 1366.
14. Yang, Z. G.; Zhang, Z. S.; Tao, Y. J.; Mai, K. C. J Appl Polym Sci 2009, 112, 1.
15. Marco, C.; Ellis, G.; Gómez, M. A.; Fatou, J. G.; Arribas, J. M.; Campoy, I.; Fontecha, A. J Appl Polym Sci 1997, 65, 2665.
16. Gróf, I.; Ďurčová, O.; Jambrich, M. Colloid Polym Sci 1992, 270, 22.
17. Laurens, C.; Ober, R.; Creton, C.; Léger, L. Macromolecules 2001, 34, 2932.
18. Laurens, C.; Ober, R.; Creton, C.; Léger, L. Macromolecules 2004, 37, 6806.
19. Varga, J.; Menyhárd, A. Macromolecules 2007, 40, 2422.
20. Olley, R. H.; Bassett, D. C. Polymer 1982, 23, 1707.
21. Jones, A. T.; Aizlewood, J. M.; Beckett, D. R. Angew Makromol Chem 1964, 75, 134.
22. Varga, J. J Macromol Sci Phys 2002, 41, 1121.
23. Bai, H. W.; Wang, Y.; Zhang, Z. J.; Han, L.; Li, Y. L.; Liu, L.; Zhou, Z. W.; Men, Y. F. Macromolecules 2009, 42, 6647.
24. Aboulfaraj, M.; G'Sell, C.; Ulrich, B.; Dahoun, A. Polymer 1995, 36, 731.
25. Luo, F.; Geng, C. Z.; Wang, K.; Deng, H.; Chen, F.; Fu, Q.; Na, B. Macromolecules 2009, 42, 9325.
26. Dong, M.; Guo, Z. X.; Yu, J.; Su, Z. Q. J Polym Sci Part B: Polym Phys 2009, 47, 314.